https://doi.org/10.5194/egusphere-2026-6956
Preprint. Discussion started: 23 November 2026
© Author(s) 2026. CC BY 4.0 License.

Warming and nutrient regime reorganize phytoplankton communities under low-silicate conditions

Yanqun Yang[a], Ziwei Yao[a], Wenjun Yao[a], Gongbo Ma[a], Yafang Li[a], Meng Cui[b], Nan Zheng[a *]

[a]National Marine Environmental Monitoring Center, Ministry of Ecological Environment, Dalian 116023, China

[b]Liaoning Hongyuanhe Nuclear Power Co., Ltd.

[*]**Corresponding author:** Nan Zheng, nzheng@nmemc.org.cn

Abstract

Coastal phytoplankton communities exposed to warming often experience concurrent changes in nutrient supply, yet their combined effects under low-silicate conditions remain poorly understood. Surface seawater collected near a thermal discharge outlet in eastern Liaodong Bay was used in a temperature and nutrient manipulation experiment to examine phytoplankton biomass dynamics, dominant group composition, and size structure. Peak chlorophyll *a* (Chl *a*) was primarily associated with nutrient supply, whereas warmer treatments generally reached peak biomass earlier, indicating that nutrient availability and temperature associated with different aspects of biomass accumulation. Community composition also varied markedly across temperature and nutrient regimes. Dinoflagellates remained numerically dominant under nutrient-poor conditions across temperatures, whereas chlorophytes and cryptophytes became dominant under warmer, phosphorus-enriched conditions.

https://doi.org/10.5194/egusphere-2026-6956
Preprint. Discussion started: 23 November 2026
© Author(s) 2026. CC BY 4.0 License.

These taxonomic changes were accompanied by a shift in Chl *a* toward the 0.7–3 μm size fraction and by changes in picophytoplankton abundance. *Synechococcus* and some eukaryotic picophytoplankton were consistent in size with potential contributions to this fraction, whereas the synchronous increase in *Prochlorococcus* more likely reflected co-variation with temperature and dissolved inorganic phosphorus rather than direct contribution. The results suggest that under low-silicate conditions, warming and nutrient regime may reorganize phytoplankton communities across biomass, taxonomic, and size dimensions, highlighting ecological responses that may not be captured by total Chl *a* alone. These findings are relevant to thermal-discharge assessment and other nutrient-altered coastal waters experiencing warming.

Keywords: warming; nutrient regime; silicon limitation; phytoplankton; size structure; thermal discharge

1. Introduction

Nuclear and thermal power plants generate large amounts of cooling water that is discharged into adjacent seas as thermal effluent, creating localized and persistent warming zones that alter the temperature field of receiving waters (Lin et al., 2021; Chen et al., 2025a). Coastal waters simultaneously experience changes in nutrient loading and stoichiometry (Malone and Newton, 2020; Park et al., 2023). Because phytoplankton form the base of marine food webs, changes in their biomass, taxonomic composition, and size structure can propagate through material cycling and

https://doi.org/10.5194/egusphere-2026-6956
Preprint. Discussion started: 23 November 2026
© Author(s) 2026. CC BY 4.0 License.

trophic transfer (Liu et al., 2023). Understanding how warming and nutrient regime act together is therefore relevant both to general coastal-ecosystem responses to environmental change and to ecological assessment of thermal-discharge areas.

The effect of temperature on phytoplankton growth is nonlinear. Below a taxon-specific thermal optimum, warming can accelerate enzymatic reactions and cell division, whereas physiological performance declines beyond the optimum (Chen, 2015; Anderson et al., 2021). Thermal response curves differ among functional groups, so warming can redistribute competitive advantages within mixed communities rather than favoring one broad taxonomic group universally (Anderson et al., 2021; Weng et al., 2025). These responses also depend on resource supply: warming effects on community growth can be stronger under nutrient-replete conditions, whereas nutrient limitation can constrain the extent to which higher temperature translates into greater production (Thomas et al., 2017; Anderson et al., 2022).

Changes in nutrient supply also profoundly affect phytoplankton community structure. Concentrations and ratios of nitrogen, phosphorus, and silicon regulate resource limitation and competitive outcomes. Silicon is required for diatom frustule formation, and declining silicate availability can shift communities away from diatom dominance (Zhou et al., 2017). High N:P conditions can favor taxa capable of exploiting alternative phosphorus pools or maintaining growth at low inorganic phosphorus availability (Zheng et al., 2023; Ou et al., 2024). In some nutrient-addition experiments, diatom relative abundance has been highest when N:P approached the Redfield ratio, although this pattern is context dependent (Zhang et al.,

https://doi.org/10.5194/egusphere-2026-6956
Preprint. Discussion started: 23 November 2026
© Author(s) 2026. CC BY 4.0 License.

2019). Temperature–nutrient interactions can likewise vary with nutrient concentration and stoichiometry (Gerhard et al., 2019).

The above studies provide an important basis for understanding the joint regulation of phytoplankton communities by temperature and nitrogen and phosphorus nutrients. However, existing knowledge of temperature–nutrient interactions is mostly based on conditions with sufficient silica or without explicit manipulation of silica (Happe et al., 2024; Bi et al., 2021). For example, a systematic literature map by Happe et al. (2024) showed that among the 86 experimental designs included, only about 15% manipulated nutrient supply conditions, and none used silicon limitation as an initial culture condition. In their competition experiment between diatoms and dinoflagellates, Bi et al. (2021) added silicate to all treatments to ensure that silicon was not a limiting factor. In long-term observations in the East China Sea, Xiao et al. (2018) did not include silicate in their statistical models because silicon is generally not limiting in that region.

Low silicate availability is a long-term or seasonal feature of many coastal systems. River regulation and imbalanced nutrient inputs can lower dissolved silicon delivery and reduce Si:N and Si:P ratios, thereby weakening the competitive position of diatoms relative to non-diatom taxa (Kranzler et al., 2019; Maavara et al., 2020; Tong et al., 2023). Under such conditions, responses to warming and nitrogen–phosphorus enrichment may differ from those observed when silicate is abundant because the group that often benefits most from nutrient enrichment—diatoms—may already be resource constrained.

https://doi.org/10.5194/egusphere-2026-6956
Preprint. Discussion started: 23 November 2026
© Author(s) 2026. CC BY 4.0 License.

This study used surface seawater from the eastern coast of Liaodong Bay, an area affected by thermal discharge from a nuclear power plant. Spring waters in the area are characterized by very low phosphate and low silicate relative to dissolved inorganic nitrogen, providing a natural low-silicate background for testing temperature and nutrient effects. The sampled water mass had been exposed to the thermal-discharge environment for approximately three years before collection. Such exposure may have influenced the starting community.

To address these knowledge gaps, we asked three questions under a low-silicate background: (1) How do temperature and nutrient regime affect phytoplankton biomass dynamics? (2) How do temperature and nutrient conditions shape phytoplankton community composition under low-silicate conditions? (3) How are changes in phytoplankton community composition related to size structure and picophytoplankton abundance?

These questions were addressed through an incubation experiment manipulating temperature and nutrient conditions using a natural coastal phytoplankton assemblage. The analysis focused on three linked response levels, including Chl a accumulation dynamics, dominant group composition near peak biomass, and size fractionated Chl a. The thermal discharge site was treated primarily as the environmental context from which the experimental community was obtained. This framing enables the results to be interpreted more broadly in relation to warming and nutrient effects in low silicate coastal waters.

https://doi.org/10.5194/egusphere-2026-6956
Preprint. Discussion started: 23 November 2026
© Author(s) 2026. CC BY 4.0 License.

2. Material and methods

2.1 Study area and experimental design

The experimental seawater was collected from the eastern coast of Liaodong Bay in the Bohai Sea, a coastal area influenced by thermal discharge from a nearby nuclear power plant (Fig. 1). Field surveys in 2025 showed pronounced local thermal gradients within the thermal discharge area, with surface temperatures ranging from 10.8 to 18.8 °C in spring and from 24.0 to 33.0 °C in summer, corresponding to spatial temperature differences of 8.0 and 9.0 °C, respectively (Fig. S1). Spring surveys also showed particularly low DIP and DSi concentrations, providing the environmental background for the incubation experiment. Surface seawater for the experiment was collected on 15 April 2025 at 121.47°E, 39.78°N, near the thermal discharge outlet.

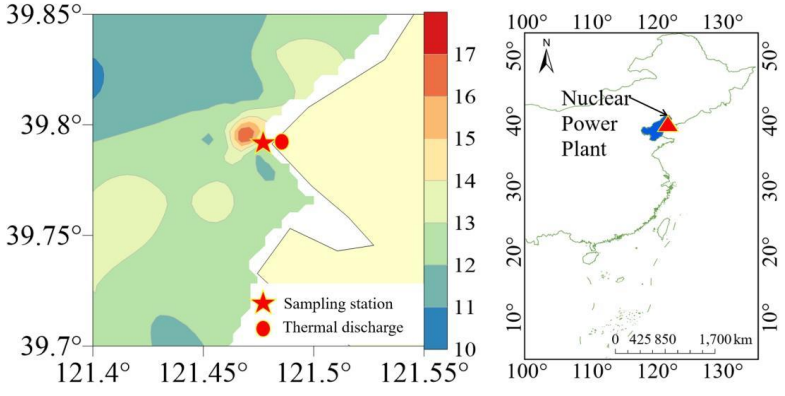


Fig. 1 Sampling station locations within the study area and the water temperature of the sampling area.

To investigate the combined effects of temperature and nutrient regime on

https://doi.org/10.5194/egusphere-2026-6956
Preprint. Discussion started: 23 November 2026
© Author(s) 2026. CC BY 4.0 License.

phytoplankton communities, surface seawater was collected on 15 April 2025 near a nuclear power plant thermal discharge outlet in eastern Liaodong Bay at 121.47°E, 39.78°N (Fig. 1). The water was prefiltered through a 200 mesh sieve with a 75 μm aperture to remove large zooplankton and debris while retaining the natural microbial and small plankton assemblage. The filtered water was dispensed into 20 L transparent polycarbonate incubation bottles at a filling volume of 18 L per bottle, with two replicate bottles per treatment. Bottles were placed in temperature controlled water baths, and temperature was regulated to ±0.5 °C.

Four temperature levels were selected from field observations of the thermal-discharge temperature range: 16 °C (ambient), 20 °C (+4 °C), 24 °C (+8 °C), and 26 °C (+10 °C). The 20 and 24 °C treatments represented warming within the range encountered near the discharge zone, whereas 26 °C was used as the upper experimental temperature (Fig. S1).

Nutrient enrichment was based on the measured background concentrations of dissolved inorganic nitrogen (DIN), dissolved inorganic phosphorus (DIP), and dissolved silicate (DSi). Three nutrient treatments were established: Ambient (no nutrient addition), Balanced DIN:DIP (target DIN:DIP = 16:1; realized initial DIN:DIP = 9.5–12.0:1), and High DIN:DIP, which created a strongly phosphorus-deficient nutrient regime (target DIN:DIP = 100:1; realized initial DIN:DIP = 82.1–132.7:1). Stock solutions of $NaNO_3$ and KH_2PO_4 were used to adjust DIN and DIP. No silicate was added. The design therefore manipulated nutrient regime, including phosphorus availability, total nutrient supply, and DIN to DIP

https://doi.org/10.5194/egusphere-2026-6956
Preprint. Discussion started: 23 November 2026
© Author(s) 2026. CC BY 4.0 License.

146 stoichiometry, rather than isolating the effect of DIN:DIP alone. Initial chemistry is
147 summarized in Table 1.

148 The incubation lasted for 31 days under natural light conditions.
149 Photosynthetically active radiation was not measured. The bottles were kept upright
150 and sealed with gas permeable membranes that allowed gas exchange while
151 minimizing evaporative loss. Each bottle was manually shaken three times daily.
152 Samples were collected for Chl *a*, nutrients, phytoplankton community composition,
153 picophytoplankton, and bacterial abundance. Sampling was conducted daily from day
154 0 to day 10 and subsequently on days 12, 14, 19, 26, and 31. The cumulative sampling
155 volume remained below two thirds of the initial incubation volume. The lower
156 sampling frequency after day 10 should be considered when interpreting late peak
157 timing because temporal resolution was reduced during this phase.

158 Table 1. Initial nutrient conditions across temperature and nutrient treatments (mean ± sample
159 standard deviation, n = 2 replicate bottles).

T (°C)	Treatment	DIN (μmol·L^{-1})	DIP (μmol·L^{-1})	DSi (μmol·L^{-1})	DIN:DIP (molar ratio)	DSi:DIN (molar ratio)
16	Ambient	11.59 ± 2.93	0.0010 ± 0.0004	0.54 ± 0.25	—	0.0468
16	Balanced DIN:DIP	68.92 ± 5.41	5.95 ± 0.48	0.43 ± 0.14	11.6	0.0062
16	High DIN:DIP	61.91 ± 4.75	0.47 ± 0.13	1.89 ± 2.30	132.7	0.0305
20	Ambient	12.39 ± 5.00	0.0160 ± 0.0221	3.34 ± 0.35	—	0.2698
20	Balanced DIN:DIP	56.08 ± 14.55	4.66 ± 1.03	0.25 ± 0.01	12.0	0.0045
20	High DIN:DIP	41.85 ± 1.31	0.51 ± 0.02	2.32 ± 1.86	82.1	0.0554
24	Ambient	9.17 ± 0.83	trace	trace	—	—
24	Balanced DIN:DIP	46.76 ± 0.68	4.91 ± 0.61	0.06 ± 0.09	9.5	0.0014
24	High DIN:DIP	55.52 ± 6.73	0.52 ± 0.09	1.30 ± 1.83	106.8	0.0233
26	Ambient	10.13 ± 0.33	0.0019 ± 0.0003	0.53 ± 0.89	—	0.0523
26	Balanced DIN:DIP	52.88 ± 0.87	4.63 ± 1.05	trace	11.4	—
26	High DIN:DIP	48.47 ± 0.53	0.45 ± 0.06	0.55 ± 0.67	106.6	0.0113

https://doi.org/10.5194/egusphere-2026-6956
Preprint. Discussion started: 23 November 2026
© Author(s) 2026. CC BY 4.0 License.

Note: DIN is the sum of nitrate, nitrite, and ammonium. Molar ratios were calculated from mean concentrations. DIN:DIP was not reported for Ambient treatments because DIP was at trace concentrations. “Trace” denotes a blank-corrected value at or below the reliable quantification range. DSi:DIN was not calculated when DSi was trace.

https://doi.org/10.5194/egusphere-2026-6956
Preprint. Discussion started: 23 November 2026
© Author(s) 2026. CC BY 4.0 License.

2.2 Sample collection and analytical methods

Field surveys were conducted in spring and summer of 2025. Surface and bottom seawater samples were collected using a polymethyl methacrylate water sampler. Water temperature, salinity, and depth were measured *in situ* with a conductivity-temperature-depth (CTD) profiler.

For nutrient analysis, seawater samples were filtered through a 0.45 μm cellulose acetate membrane. The filtrate was transferred into polyethylene bottles and stored at –20°C. Concentrations of nitrate, nitrite, ammonium, phosphate, and silicate were determined by flow analysis (Grasshoff et al., 1999; Becker et al., 2020). Nitrite was measured by the diazo-coupling reaction, nitrate was reduced to nitrite through a cadmium column and then measured by the same method, ammonium was analyzed by the indophenol blue method, phosphate was determined by the phosphomolybdenum blue method, and silicate was measured by the silicomolybdenum blue method.

Chl *a* samples were size-fractionated by sequential filtration through a 20 μm nylon membrane, a 3 μm polycarbonate membrane, and a 0.7 μm GF/F glass fiber filter, yielding the >20 μm, 3–20 μm, and 0.7–3 μm fractions, respectively. Filter was folded, wrapped in aluminum foil, and stored at –20°C. Pigments were extracted in 90% acetone at 4 °C in darkness for 12–24 h and quantified fluorometrically (excitation 430 nm, emission 670 nm) using a Chl *a* standard for calibration (Holm-Hansen et al., 1965; Lysenko et al., 2022).

https://doi.org/10.5194/egusphere-2026-6956
Preprint. Discussion started: 23 November 2026
© Author(s) 2026. CC BY 4.0 License.

For phytoplankton community analysis, 250 mL of seawater was collected in each bottle and immediately fixed with Lugol's solution (final concentration approximately 1%). The samples were stored at room temperature in the dark. In the laboratory, they were left to settle for 24 to 48 hours and then concentrated to about 50 mL. A 0.1 mL subsample was placed into a 0.1 mL counting chamber, and species identification and cell counting were performed under an optical microscope at 200–400× magnification (Utermöhl, 1958; Tomas, 1997).

Picophytoplankton samples were collected in 2 mL aliquots, fixed immediately, and stored at −80 °C until analysis. Samples were analyzed using a flow cytometer equipped with a 488 nm laser. Eukaryotic picophytoplankton, *Synechococcus*, and *Prochlorococcus* were identified according to their characteristic forward scatter, side scatter, and orange and red autofluorescence signals. For each sample, 10,000 to 50,000 events were recorded, and fluorescent microspheres were used for instrument calibration. Cell abundances were expressed as $\times 10^4$ cells·mL^{-1} (Marie et al., 1997; Thyssen et al., 2023).

Quality control was maintained throughout the analysis using field blanks, duplicate samples, spiked recovery tests, and certified reference materials. For nutrient analysis, recovery rates were controlled between 85% and 115%, and the relative deviation of duplicates was kept below 5%. Chl *a* analysis was calibrated with a Chl *a* standard, and the relative deviation of duplicates was maintained below 10%. Phytoplankton identification and counting were performed by a single analyst to ensure consistency in taxonomic criteria.

https://doi.org/10.5194/egusphere-2026-6956
Preprint. Discussion started: 23 November 2026
© Author(s) 2026. CC BY 4.0 License.

2.3 Statistical analysis

The first Chl *a* peak day and the two preceding sampling days were used as the analysis window, yielding 36 observations across 12 temperature–nutrient combinations. Because environmental variables were constant within each combination, the number of independent environmental units was 12, and significance should be interpreted under this constraint. Two redundancy analysis (RDA) steps were performed. First, temperature, DIN, DIP and DSI were explanatory variables for the proportions of three size-fractionated Chl *a* fractions (>20, 3–20, 0.7–3 μm). Second, size structure was added as an explanatory variable for the relative abundances of four phytoplankton groups (diatoms, dinoflagellates, chlorophytes, cryptophytes) and the absolute abundances of three picophytoplankton groups. Picophytoplankton abundances were log10-transformed after adding 0.01 because they spanned several orders of magnitude and contained zeros.

Because the three size fractions and the four phytoplankton groups each summed to 100%, direct inclusion in RDA would introduce perfect collinearity. A centered log-ratio (CLR) transformation was applied to each set of proportions. CLR coordinates are not mutually independent (rank D−1); therefore, CLR was used for univariate Spearman correlations, whereas only D−1 coordinates were retained in RDA (two for size fractions, three for phytoplankton groups) to avoid residual collinearity. All variables were z-score standardized. Spearman correlations tested monotonic relationships, and RDA quantified variance explained by environmental factors. The global RDA model and each environmental variable were tested with 999

https://doi.org/10.5194/egusphere-2026-6956
Preprint. Discussion started: 23 November 2026
© Author(s) 2026. CC BY 4.0 License.

free permutations; because the number of independent units was 12, *P* values should be interpreted conservatively. No multiple-comparison correction was applied to Spearman correlations, as these analyses were exploratory. Sensitivity analyses using only the peak day and excluding samples with large matching offsets were performed. Analyses were conducted in R 4.4.1 using vegan, ggplot2 and ggrepel.

3. Results

3.1 Biomass accumulation dynamics and nutrient depletion

Peak Chl *a* concentrations exhibited clear gradients among nutrient treatments, corresponding to the initial nutrient supply levels. In the Balanced DIN:DIP treatment, peak Chl *a* ranged from 21.82 to 31.16 μg·L^{-1} across temperatures, representing the highest values among all treatments. In the High DIN:DIP treatment, peak Chl *a* ranged from approximately 9.0 to 19.5 μg·L^{-1}, approximately 40–65% of those in the Balanced DIN:DIP treatment. In the Ambient treatment, peak Chl *a* was the lowest among all treatments (approximately 2–4 μg·L^{-1}). Overall, peak biomass exhibited a clear trend of increasing with initial nitrogen and phosphorus supply levels.

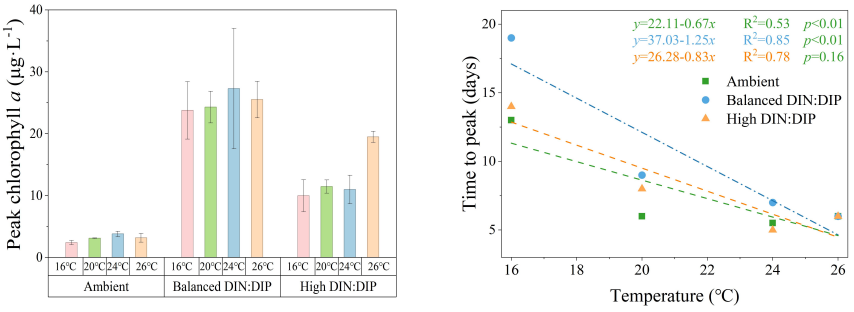
Within each nutrient treatment, peak biomass did not differ significantly among temperatures. In the Balanced DIN:DIP treatment, peak Chl *a* remained similar across the four temperature levels (one-way ANOVA, $F_{3,4} = 1.36$, $p = 0.375$), indicating no statistically detectable temperature effect on the biomass ceiling under this experimental design. In the High DIN:DIP treatment, the temperature effect was also not significant, although the mean peak at 26 °C (approximately 19 μg·L^{-1}) was

https://doi.org/10.5194/egusphere-2026-6956
Preprint. Discussion started: 23 November 2026
© Author(s) 2026. CC BY 4.0 License.

higher than at lower temperatures (approximately 9–11 μg·L^{-1}). In the Ambient treatment, the temperature effect was not significant either. Collectively, under the same nutrient conditions, peak biomass converged across temperatures, indicating that warming did not significantly alter the biomass ceiling set by nutrient supply.

In contrast to the lack of a detectable temperature effect on peak biomass, the time required to reach the peak exhibited a strong response to warming. In the Balanced DIN:DIP treatment, the time to peak decreased progressively from 19 days at 16 °C to 9 days at 20 °C, 7 days at 24 °C, and 6 days at 26 °C, with linear regression confirming a significant negative relationship between peak time and temperature. A similar decreasing trend was observed in the High DIN:DIP treatment, with peak time decreasing from 14 days at 16 °C to 8 days at 20 °C, 5 days at 24 °C, and 6 days at 26 °C, although the linear relationship was not significant. In the Ambient treatment, peak time also decreased significantly with temperature, from 13 days at 16 °C to 6 days at 20 °C, 5.5 days at 24 °C, and 6 days at 26 °C. Notably, peak times stabilized at 5–7 days within the 24–26 °C range across all treatments, suggesting possible saturation of the temperature-acceleration effect near the upper end of the thermal gradient.

https://doi.org/10.5194/egusphere-2026-6956
Preprint. Discussion started: 23 November 2026
© Author(s) 2026. CC BY 4.0 License.



268 Fig. 2 Peak chlorophyll *a* (Chl *a*) concentration and time to reach peak under different
269 temperature and nutrient treatments.

270 3.2 Peak-phase dominant groups and community succession

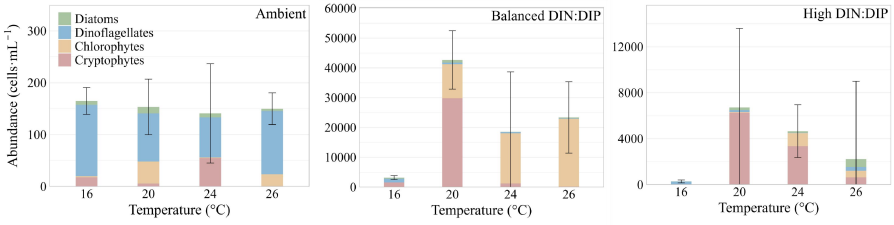
271 At the early incubation stage, total phytoplankton abundance in all treatment
272 groups was extremely low (0–52.5 cells·mL^{-1}), with Dinoflagellates, Cryptophytes,
273 Chlorophytes, and Diatoms all present across different groups. On the peak day, the
274 response of dominant taxa appeared stronger to nutrient treatments than to
275 temperature. In the Ambient group, Dinoflagellates were the dominant taxa at all
276 temperatures (approximately 55%–83%); only at 24°C did the proportion of
277 Cryptophytes increase to about 39%, but this did not change the overall dominance
278 pattern. In the Balanced DIN:DIP group, dominant taxa showed a clear succession
279 with temperature: at 16°C, Cryptophytes and Dinoflagellates were co-dominant
280 (approximately 49% and 40%); at 20°C, Cryptophytes became overwhelmingly
281 dominant (approximately 70%), with Chlorophytes increasing to about 27%; at 24°C
282 and 26°C, Chlorophytes became dominant, accounting for approximately 91% and
283 97%, respectively. In the High DIN:DIP group, Dinoflagellates dominated at 16°C

https://doi.org/10.5194/egusphere-2026-6956
Preprint. Discussion started: 23 November 2026
© Author(s) 2026. CC BY 4.0 License.

(approximately 90%); Cryptophytes dominated at both 20°C and 24°C (approximately 93% and 72%), with Chlorophytes being subdominant at 24°C (approximately 25%); at 26°C, dominance was more evenly distributed, with Diatoms, Cryptophytes, Chlorophytes, and Dinoflagellates accounting for approximately 31%, 29%, 26%, and 15%, respectively.

At the same temperature, comparisons showed that at 16°C, Dinoflagellates dominated in both the Ambient and High DIN:DIP groups, whereas Cryptophytes and Dinoflagellates were co-dominant in the Balanced DIN:DIP group; at 20°C, Dinoflagellates still dominated in the Ambient group, while Cryptophytes became dominant in both the Balanced DIN:DIP and High DIN:DIP groups, although Chlorophytes were more clearly subdominant in the Balanced DIN:DIP group; at 24°C, the three groups diverged most strongly, with Dinoflagellates dominating in Ambient, Chlorophytes in Balanced DIN:DIP, and Cryptophytes in High DIN:DIP; at 26°C, Dinoflagellates still dominated in Ambient, Chlorophytes were overwhelmingly dominant in Balanced DIN:DIP, and multiple taxa were relatively balanced in High DIN:DIP. Overall, changes in nutrient ratios were the main factor associated with shifts in dominant taxa on the peak day: Balanced DIN:DIP was associated with Chlorophyte dominance at 24–26°C, High DIN:DIP promoted Cryptophyte dominance at 20–24°C, whereas under Ambient conditions, temperature variation had relatively little effect on dominant taxa.

https://doi.org/10.5194/egusphere-2026-6956
Preprint. Discussion started: 23 November 2026
© Author(s) 2026. CC BY 4.0 License.



304 Fig. 3 Peak-day phytoplankton community composition and abundance across
305 temperatures under Ambient, Balanced DIN:DIP, and High DIN:DIP treatments.

306 3.3 Size structure and picophytoplankton composition

307 At the time of peak biomass, size structure and picophytoplankton community
308 composition differed among nutrient treatments (Fig. 4).

309 In terms of size structure, the contribution of the 0.7–3 μm fraction to total Chl *a*
310 increased markedly with temperature in the Balanced DIN:DIP treatment, from 42.7%
311 at 16°C to 84.0% at 20°C, and 74.9% and 73.7% at 24°C and 26°C, respectively.
312 Correspondingly, the contributions of the >20 μm and 3–20 μm fractions decreased;
313 the >20 μm proportion declined from 9.8% at 16°C to 2.9% at 26°C, and the 3–20 μm
314 proportion decreased from 47.4% to 23.4%. In the High DIN:DIP treatment, the 0.7–3
315 μm proportion also increased with temperature (16°C: 34.3%; 20–26°C: 67.0–73.5%),
316 but the increase was slightly lower than in the Balanced DIN:DIP treatment. In the
317 Ambient treatment, the 0.7–3 μm proportion fluctuated among temperatures
318 (35.3–53.6%) and showed no consistent temperature trend.

319 The taxonomic composition of picophytoplankton was generally consistent with
320 the changes in size structure. In the Balanced DIN:DIP treatment, both
321 *Prochlorococcus* and eukaryotic picophytoplankton increased with temperature.

https://doi.org/10.5194/egusphere-2026-6956
Preprint. Discussion started: 23 November 2026
© Author(s) 2026. CC BY 4.0 License.

Prochlorococcus increased from 0.08×10^4 cells·mL^{-1} at 16°C to 3.82×10^4 cells·mL^{-1} at 26°C, while eukaryotic picophytoplankton increased from 0.598×10^4 at 16°C to 2.23×10^4 at 24°C, and slightly decreased to 2.07×10^4 cells·mL^{-1} at 26°C. *Synechococcus* showed no consistent temperature trend. In the High DIN:DIP treatment, *Prochlorococcus* peaked at 20°C (2.32×10^4 cells·mL^{-1}), decreased to 0.29×10^4 at 24°C, and rose to 1.14×10^4 cells·mL^{-1} at 26°C; eukaryotic picophytoplankton were highest at 20°C and lower at other temperatures. In the Ambient treatment, all picophytoplankton groups had low abundances and showed no consistent temperature trend.

The synchronous variation between 0.7–3 μm Chl *a* concentration and *Prochlorococcus* abundance was most pronounced in the Balanced DIN:DIP treatment. Both increased with temperature; 0.7–3 μm Chl *a* increased from 8.76 μg·L^{-1} at 16°C to 18.8 μg·L^{-1} at 26°C, and *Prochlorococcus* increased from 0.08×10^4 cells·mL^{-1} to 3.82×10^4 cells·mL^{-1}. The increase in Chl *a* in this size fraction corresponded to the expansion of *Prochlorococcus*. In the High DIN:DIP and Ambient treatments, the correspondence between 0.7–3 μm Chl *a* and *Prochlorococcus* was not evident.

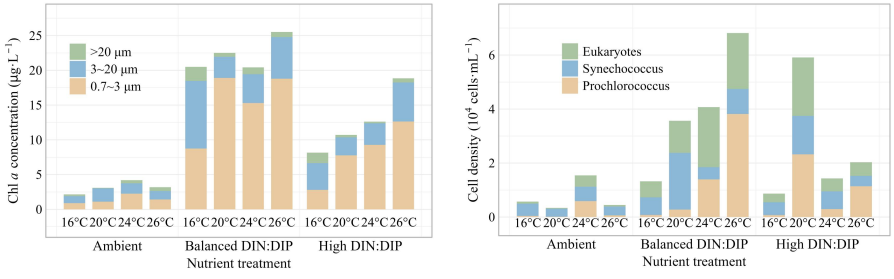


Fig. 4 Size-fractionated chlorophyll *a* (Chl *a*) composition and picophytoplankton

https://doi.org/10.5194/egusphere-2026-6956
Preprint. Discussion started: 23 November 2026
© Author(s) 2026. CC BY 4.0 License.

abundance at peak biomass under different temperature and nutrient treatments.

3.4 Relationships of community and size structure with environmental factors

Temperature and DIP were jointly associated with the shift of Chl *a* toward smaller size fractions. Temperature was significantly positively correlated with the 0.7–3 μm fraction (r = 0.47, P = 0.004) and negatively correlated with the >20 μm fraction (r = −0.48, P = 0.003). DIP was significantly positively correlated with the 0.7–3 μm fraction (r = 0.61, P < 0.001) and negatively correlated with the >20 μm fraction (r = −0.51, P = 0.001). DSI was significantly negatively correlated only with the >20 μm fraction, while DIN showed no significant relationship with any size fraction. RDA confirmed the relative importance of these factors in the same order: DIP (P = 0.001), the 3–20 μm component (P = 0.004) and temperature (P = 0.045) were significant, whereas DIN, DSI and the >20 μm component were not.

This shift in size structure was closely synchronized with the reorganization of community composition. DIP was the strongest driver of community composition, showing a significant positive correlation with the relative abundance of chlorophytes (r = 0.69, P = 0.003), and temperature was likewise significantly positively correlated with chlorophytes (r = 0.53, P = 0.035). On the RDA1 axis, temperature and DIP clustered at the negative end together with chlorophytes and cryptophytes, while dinoflagellates and diatoms occupied the positive end. This indicates that warm, phosphorus-rich conditions simultaneously were associated with higher/lower relative abundances, so that community reorganization and size miniaturization represent two

https://doi.org/10.5194/egusphere-2026-6956
Preprint. Discussion started: 23 November 2026
© Author(s) 2026. CC BY 4.0 License.

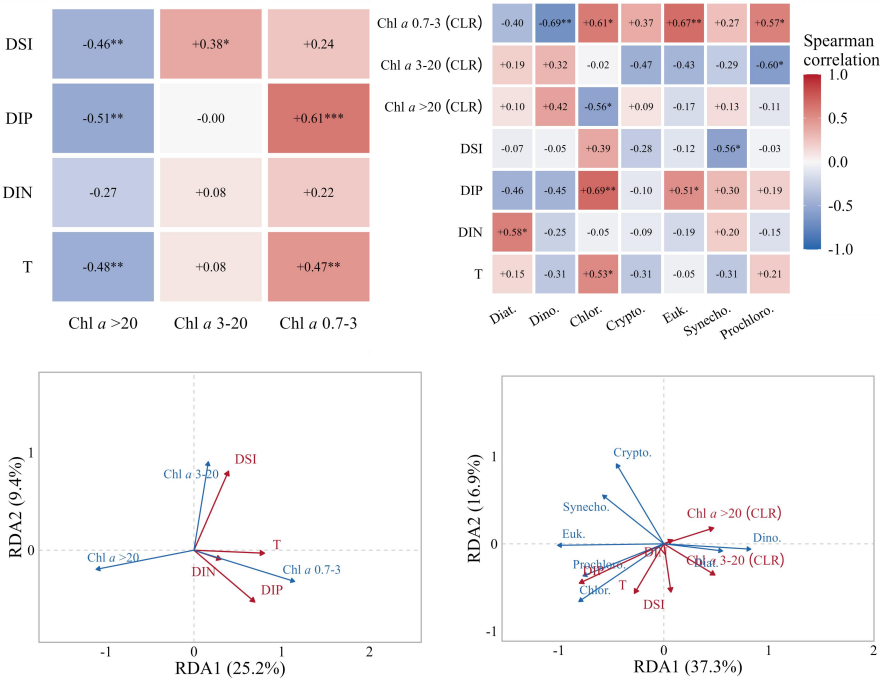
facets of the same process.

The correspondence between size structure and picophytoplankton groups was also evident. The 0.7–3 μm component was significantly positively correlated with the absolute abundance of eukaryotic picophytoplankton (r = 0.67, P = 0.004) and *Prochlorococcus* (r = 0.57, P = 0.020), indicating that the expansion of the small size fraction was partly contributed by the growth of picophytoplankton. This component was significantly negatively correlated with the relative abundance of dinoflagellates (r = −0.69, P = 0.003) and positively correlated with chlorophytes (r = 0.61, P = 0.013). The 3–20 μm component was significantly negatively correlated with *Prochlorococcus* (r = −0.60, P = 0.014), and the >20 μm component was significantly negatively correlated with chlorophytes (r = −0.56, P = 0.025). On the RDA1 axis, eukaryotic picophytoplankton, *Prochlorococcus* and *Synechococcus* clustered at the negative end together with temperature and DIP, while the 3–20 μm component, dinoflagellates and diatoms occupied the positive end, indicating that size structure, picophytoplankton abundance and phytoplankton composition co-varied along a single environmental gradient.

The overall RDA model was significant (F = 2.90, P = 0.002), with environmental factors and size structure together explaining 65.9% of the variation in community composition and picophytoplankton abundance, of which RDA1 accounted for 37.3%. The directions of significant correlations in the correlation analysis were fully consistent with the RDA loadings, so that the two analytical approaches corroborated each other and jointly revealed a consistent pattern of

https://doi.org/10.5194/egusphere-2026-6956
Preprint. Discussion started: 23 November 2026
© Author(s) 2026. CC BY 4.0 License.

383 covariation among temperature and DIP, size structure, community composition, and
384 picophytoplankton abundance.



385 Fig. 5 Correlation and redundancy analysis (RDA) showing the relationships among
386 environmental factors, size-fractionated chlorophyll *a* (Chl *a*), and phytoplankton
387 community composition at the peak window. Abbreviations: Chl *a*, chlorophyll *a*;
388 CLR, centered log-ratio; DIN, dissolved inorganic nitrogen; DIP, dissolved inorganic
389 phosphorus; DSI, dissolved silicate; Diat., diatoms; Dino., dinoflagellates; Chlor.,
390 chlorophytes; Crypto., cryptophytes; Euk., eukaryotic picophytoplankton; Synecho.,
391 *Synechococcus*; Prochloro., *Prochlorococcus*.

https://doi.org/10.5194/egusphere-2026-6956
Preprint. Discussion started: 23 November 2026
© Author(s) 2026. CC BY 4.0 License.

4. Discussion

4.1 Nutrient supply sets peak Chl *a* and temperature regulates time to peak

In this experiment, peak Chl *a* differed markedly among nutrient treatments but varied little with temperature within the same nutrient treatment, whereas the time to peak decreased significantly with increasing temperature and stabilized at 24–26 °C (Fig. 2). The contrasting responses of peak Chl *a* and time to peak to nutrient and temperature suggest that these two variables may be governed by distinct processes. Peak Chl *a* was primarily associated with nutrient supply level, while time to peak was primarily associated with temperature.

Peak Chl *a* was constrained by nutrient supply. As the availability of limiting nutrients became insufficient to sustain further biomass accumulation, the peak was primarily associated with the initial total nutrient supply (Frank et al., 2020; Happe et al., 2024; Fig. 2). Under nutrient-replete conditions, the total available nitrogen and phosphorus were higher, resulting in a higher peak. Under nutrient-poor conditions, available resources were insufficient to support higher biomass, and even if warming accelerated physiological processes, the peak remained low. Nutrient limitation also weakened the positive effect of temperature on growth (Thomas et al., 2017), potentially preventing warming from being translated into higher biomass accumulation. The observed pattern of marked variation in peak Chl *a* among nutrient treatments but little variation with temperature is consistent with this mechanism.

Time to peak was strongly associated with temperature. Temperature is known to

https://doi.org/10.5194/egusphere-2026-6956
Preprint. Discussion started: 23 November 2026
© Author(s) 2026. CC BY 4.0 License.

accelerate enzymatic reaction rates, which may speed up photosynthesis, nutrient uptake, and cell division, and thus biomass accumulation (Barton et al., 2020; Kholssi et al., 2023). Consequently, warming allows the community to reach the nutrient-determined peak more rapidly, shortening the time to peak. However, the growth response to temperature is not monotonic. At low temperatures, warming mainly stimulates enzymatic reactions, and growth rate increases. Beyond a certain temperature, high temperature may begin to damage enzymes and membrane structures, potentially causing growth rate to decline, and respiration costs increase relatively, causing growth rate to decline (Kontopoulos et al., 2020). This means that once temperature exceeds the community's optimum, further warming no longer accelerates biomass accumulation, and the time to peak no longer decreases. In this experiment, the time to peak decreased significantly with temperature but stabilized at 24–26 °C (Fig. 2), suggesting that the temperature response of time to peak began to level off between 24 and 26 °C in this water mass, and the accelerating effect of warming on biomass accumulation tends to saturate. Under warm conditions, community composition shifted toward small and picophytoplankton taxa, which have been reported to exhibit relatively high growth rates under some environmental conditions (Anderson et al., 2021). Therefore, the shortening of the time to peak may also be partly mediated by changes in community composition.

4.2 Temperature and nutrient supply jointly shape peak phytoplankton composition

Section 4.1 showed that peak Chl *a* was mainly determined by nutrient supply

https://doi.org/10.5194/egusphere-2026-6956
Preprint. Discussion started: 23 November 2026
© Author(s) 2026. CC BY 4.0 License.

level, but communities with similar or identical total Chl *a* may differ completely in taxonomic composition. In this experiment, peak Chl *a* in the Balanced and High DIN:DIP treatments was markedly higher than in the Ambient treatment, yet the dominant groups among the three treatments did not change in the same direction across temperatures and nutrient treatments (Fig. 3). This indicates that total Chl *a* alone is insufficient to resolve the effects of temperature and nutrients on the community, and that further analysis of the taxonomic composition underlying peak Chl *a* is needed.

The core question of this experiment is which taxa can dominate numerically under the interactive effects of temperature and nutrients. Cell abundance directly reflects the proliferation efficiency of taxa and population-level competitive outcomes, whereas carbon biomass mainly reflects standing stock and is influenced by differences in cell size and carbon content; it does not directly indicate the rate of proliferation (Guo et al., 2025) . Therefore, this study defines "dominant groups" based on cell abundance, that is, taxa that dominate numerically, and this indicator is suitable for analyzing competitive dynamics.

The experimental results showed that in the Ambient treatment, dinoflagellates dominated at all temperatures, and temperature changes did not significantly alter this pattern (Fig. 3). In contrast, in the nutrient-enriched Balanced and High DIN:DIP treatments, increasing temperature shifted the dominant groups from dinoflagellates to cryptophytes or chlorophytes (Fig. 3). Correlation analysis also supported this pattern: both DIP and temperature were positively correlated with the relative abundance of

https://doi.org/10.5194/egusphere-2026-6956
Preprint. Discussion started: 23 November 2026
© Author(s) 2026. CC BY 4.0 License.

chlorophytes, and temperature, DIP, chlorophytes, cryptophytes, eukaryotic picophytoplankton, and Prochlorococcus clustered at the negative end of RDA1, whereas dinoflagellates, diatoms, the >20 μm fraction, and the 3–20 μm fraction clustered at the positive end (Fig. 5). This indicates that temperature and DIP together constituted an environmental gradient shifting from dinoflagellate dominance to chlorophyte and cryptophyte dominance.

The mechanism behind this pattern may lie in the possibility that nutrient supply level altered the nature of competition, thereby determining whether temperature could affect competitive outcomes. Under nutrient-poor conditions, competition mainly centered on the ability to acquire nutrients at low concentrations. Dinoflagellates can maintain a competitive advantage through strategies such as vertical migration to obtain deep-water nutrients (Zheng et al., 2023), release of extracellular enzymes to utilize organic phosphorus (Chen et al., 2025b), and mixotrophy (Zheng et al., 2023; Ou et al., 2024). Therefore, in this experiment, dinoflagellate dominance was not displaced by temperature changes. Under relatively nutrient-sufficient conditions, the concentration of the limiting nutrient is no longer the sole bottleneck of competition, and competition shifts to a comparison of growth rates. Different phytoplankton taxa differ in their thermal responses. Under resource-sufficient conditions, the extent to which warming promotes growth rate varies among taxa, and taxa with stronger growth-rate responses to temperature gradually gain dominance under warm conditions. In this experiment, chlorophytes and cryptophytes rapidly became dominant at 20–26 ℃, indicating that their growth

https://doi.org/10.5194/egusphere-2026-6956
Preprint. Discussion started: 23 November 2026
© Author(s) 2026. CC BY 4.0 License.

rates may respond more strongly to temperature than those of dinoflagellates, whereas the thermal reaction norm of dinoflagellates is relatively flat, with limited variation in growth rate with temperature (Anderson et al., 2021). Therefore, in the Balanced DIN:DIP treatment, as temperature increased, the growth-rate advantage of chlorophytes and cryptophytes may have become evident, and dinoflagellates were associated with a decline in dominance.

In the High DIN:DIP treatment, phosphorus limitation weakened the response of chlorophytes to warming to some extent, and cryptophytes became the main dominant group. This difference is consistent with the positive correlation between DIP and chlorophytes (Fig. 5): the dominance of chlorophytes requires relatively sufficient phosphorus supply, whereas cryptophytes may have a lower dependence on phosphorus (Isanta-Navarro et al., 2024).

When N:P approaches the Redfield ratio, diatom relative abundance typically reaches its maximum (Zhang et al., 2019). However, no silicon was added in this experiment, and diatoms did not dominate in most treatments. Competition mainly occurred among dinoflagellates, cryptophytes, and chlorophytes. Silicon limitation was associated with low diatom dominance, a group that typically dominates under high-nutrient conditions (Zhou et al., 2017; Zhang et al., 2024), altering the direction of the effect of nutrient enrichment on community composition. Under silicon-replete conditions, high nutrients generally favor diatoms (Bi et al., 2021), whereas in this experiment, chlorophytes or cryptophytes dominated under high nutrient conditions.

https://doi.org/10.5194/egusphere-2026-6956
Preprint. Discussion started: 23 November 2026
© Author(s) 2026. CC BY 4.0 License.

4.3 Coupled size and community shifts under silicon limitation

Sections 4.1 and 4.2 showed that peak Chl *a* was mainly determined by nutrient supply level, whereas the dominant groups during the peak period were jointly associated with temperature and nutrients. However, changes in total Chl *a* are not independent of the internal structure of the community. In this experiment, the size partitioning of Chl *a* and taxonomic composition changed synchronously across temperature and nutrient treatments, providing an integrated picture of phytoplankton community responses, as summarized in the conceptual framework in Fig. 6.

Size structure changes were most pronounced in the nutrient-enriched treatments (Fig. 4). Temperature and DIP jointly drove the shift of Chl *a* from larger to smaller size fractions, with DIP showing a stronger association in the RDA, while DIN and DSI had weaker regulatory effects on size structure (Fig. 5). This pattern can be explained by a shift in the nature of competition. Under persistent silicon limitation, diatoms did not dominate, and the competitive advantage of large cells appeared to decline overall (Zhou et al., 2017; Zhang et al., 2024). Under nutrient-poor conditions, dinoflagellates maintained their competitive advantage through multiple nutrient-acquisition strategies, resulting in a community dominated by larger cells (Zheng et al., 2023; Ou et al., 2024; Chen et al., 2025b). Under relatively nutrient-sufficient conditions, the concentration of the limiting nutrient was no longer the sole bottleneck of competition, and differences in taxon-specific responses to temperature may have become more important in shaping community composition. Under warm conditions, the growth-rate advantage of small-celled taxa became

https://doi.org/10.5194/egusphere-2026-6956
Preprint. Discussion started: 23 November 2026
© Author(s) 2026. CC BY 4.0 License.

evident, and Chl *a* shifted toward the 0.7–3 μm fraction (Anderson et al., 2026).

Size miniaturization and community composition reorganization occurred synchronously along the same environmental gradient. Under high-temperature, high-phosphorus conditions, the proportions of chlorophytes and cryptophytes increased while those of dinoflagellates and diatoms decreased, consistent with the direction of size miniaturization. However, size fractions and taxonomic groups are not in one-to-one correspondence, and three logical points require particular attention. First, the co-directional relationship between chlorophytes and 0.7–3 μm Chl *a* is not a contribution relationship. All chlorophytes in this experiment were *Platymonas* sp. (8–20 μm), which fall within the 3–20 μm size fraction and do not contribute to 0.7–3 μm Chl *a*. Their co-directional pattern arises because both are driven by temperature and DIP and occupy similar positions in RDA space (Fig. 5). Second, the decline in the 3–20 μm fraction does not mean that chlorophytes declined. Although chlorophytes fall within the 3–20 μm fraction, the decline of other groups such as dinoflagellates within this fraction was larger, masking the increase in chlorophytes and resulting in an overall decline in the 3–20 μm fraction. Third, the lack of a significant individual correlation between picophytoplankton absolute abundance and temperature does not mean that temperature has no effect. Picophytoplankton abundance is more directly driven by size structure and DIP than by temperature itself, and its position in the RDA derives from co-variation with the 0.7–3 μm size fraction and DIP, rather than from an independent correlation with temperature (Fig. 5).

The expansion of small-sized Chl *a* occurred synchronously with changes in

https://doi.org/10.5194/egusphere-2026-6956
Preprint. Discussion started: 23 November 2026
© Author(s) 2026. CC BY 4.0 License.

picophytoplankton, but the relationship between the two requires careful interpretation. Size-fractionated Chl *a* and picophytoplankton are two independent measurement systems, and the cell sizes of picophytoplankton groups are not in one-to-one correspondence with size fractions. The cells of *Synechococcus* (approximately 0.8–1.5 μm) and some eukaryotic picophytoplankton (approximately 0.2–3 μm) fall within the 0.7–3 μm range and directly contribute to Chl *a* in this size fraction (Marañón et al., 2024). Prochlorococcus (approximately 0.5–0.7 μm) has most cells smaller than 0.7 μm, and its positive correlation with 0.7–3 μm Chl *a* more likely reflects co-variation driven by both temperature and DIP, rather than direct contribution (Marañón et al., 2024). Therefore, the expansion of 0.7–3 μm Chl *a* was likely contributed to by *Synechococcus* and some eukaryotic picophytoplankton, while the synchronous increase in Prochlorococcus reflected shared environmental drivers. RDA analysis also supports this interpretation, as temperature, DIP, size structure, and community composition shared the same driving axis, indicating that size miniaturization, taxonomic reorganization, and picophytoplankton expansion were statistically co-varied along the same gradient (Fig. 5). Under the low-silicate conditions of this experiment, diatoms may have been constrained, while warming and phosphorus enrichment were associated with an increased contribution of small-sized taxa, allowing chlorophytes, cryptophytes, eukaryotic picophytoplankton, and Prochlorococcus to occupy a larger share of the community, with the size distribution of Chl *a* shifting toward 0.7–3 μm.

https://doi.org/10.5194/egusphere-2026-6956
Preprint. Discussion started: 23 November 2026
© Author(s) 2026. CC BY 4.0 License.

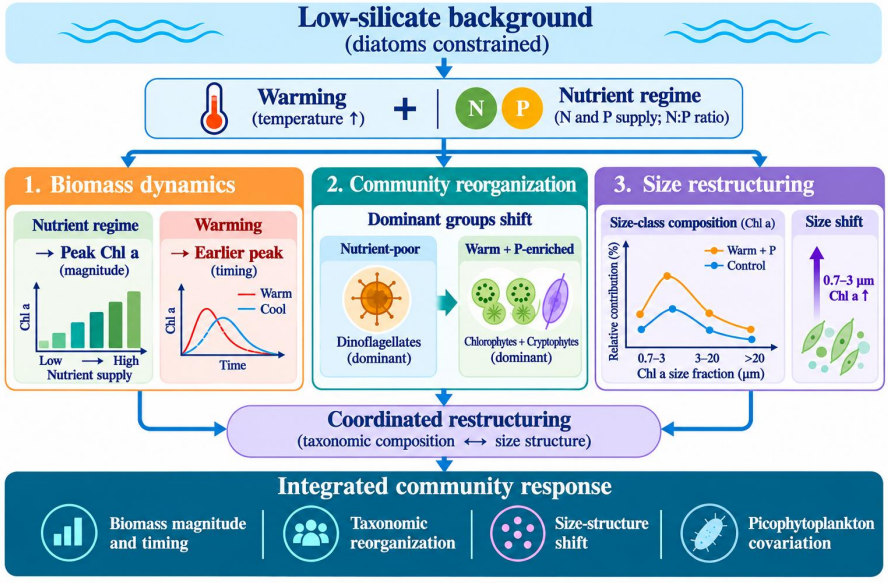


Fig. 6 Conceptual framework illustrating the coupled effects of temperature and nutrient supply on phytoplankton biomass dynamics, community reorganization, and size miniaturization under persistent silicon limitation.

For the ecological monitoring and management of thermal discharge areas, the above mechanisms have three implications. First, because the time to peak decreases with temperature, when the peak period is used as a monitoring or early warning window, the timing needs to be adjusted according to water temperature. Second, because peak Chl *a* is mainly related to nutrient supply level, the primary target for controlling peak biomass is more likely nutrient input management. Third, using total Chl *a* alone as an indicator may mask substantial changes in community composition and size structure. Under warm, nutrient-enriched conditions, an increased proportion of small-sized taxa may alter zooplankton feeding efficiency, thereby affecting energy transfer to higher trophic levels and posing a potential risk to the safety of cooling

https://doi.org/10.5194/egusphere-2026-6956
Preprint. Discussion started: 23 November 2026
© Author(s) 2026. CC BY 4.0 License.

water intake at nuclear power plants. Therefore, in monitoring thermal discharge areas, in addition to total Chl *a*, it is necessary to simultaneously monitor changes in the composition of dominant groups and size structure during the peak period (Figs. 3 and 4).

5. Conclusions

This study, conducted under persistent silicon limitation, investigated the effects of warming and nutrient input on phytoplankton communities through incubation experiments with temperature and nitrogen–phosphorus nutrient interactions. We examined three levels: Chl *a* accumulation dynamics, dominant group composition during the peak period, and size structure, revealing the mechanisms by which temperature and nutrients interact to regulate community structure. The main conclusions are as follows.

Peak Chl *a* was primarily associated with nutrient supply level, while temperature was more strongly associated with the time to peak. Warming accelerated biomass accumulation and advanced the peak, but did not significantly alter the peak level associated with nutrient supply.

Dominant groups during the peak period were jointly regulated by temperature and nutrients. Under nutrient-poor Ambient conditions, dinoflagellates dominated at all temperatures; under nutrient-enriched warm conditions, chlorophytes and cryptophytes replaced dinoflagellates as dominant groups, indicating that nutrient supply background may determine whether temperature can alter community

https://doi.org/10.5194/egusphere-2026-6956
Preprint. Discussion started: 23 November 2026
© Author(s) 2026. CC BY 4.0 License.

composition.

Changes in size structure occurred synchronously with community reorganization. Under warm, phosphorus-enriched conditions, Chl *a* shifted toward the 0.7–3 μm fraction, while the proportions of the >20 μm and 3–20 μm fractions decreased. Size miniaturization was closely associated with changes in picophytoplankton: *Synechococcus* and some eukaryotic picophytoplankton were likely contributors to the increase in 0.7–3 μm Chl *a*, whereas the synchronous increase in *Prochlorococcus* more likely reflected co-variation driven by temperature and DIP rather than a direct contribution to this size fraction. Temperature and DIP were jointly associated with size miniaturization, taxonomic reorganization, and picophytoplankton expansion.

Under persistent silicon limitation, the competitive advantage of diatoms was suppressed, and warming plus phosphorus enrichment further amplified the advantage of small-celled taxa. These mechanisms suggest that in similar thermal discharge-affected areas, using total Chl *a* alone as a monitoring indicator may mask substantial changes in community composition and size structure; in addition to total Chl *a*, it is necessary to simultaneously monitor changes in dominant group composition and size structure during the peak period, so as to more comprehensively assess the potential impacts of thermal discharge on phytoplankton communities and the safety of cooling water intake at nuclear power plants.

https://doi.org/10.5194/egusphere-2026-6956
Preprint. Discussion started: 23 November 2026
© Author(s) 2026. CC BY 4.0 License.

Data Availability

The data and metadata supporting the results of this study are archived in Zenodo at https://doi.org/10.5281/zenodo.23053892. The archived dataset includes a README file, a data dictionary, bottle-level peak analysis data, and peak-selection quality-control records. These data are sufficient to reproduce the analyses presented in this paper. The full experimental time-series data are not used in the analyses presented here and are available from the corresponding author upon reasonable request.

Competing interest

The authors declare no conflict of interest.

Author Contribution

Yanqun Yang: Funding acquisition, Conceptualization, Methodology, Writing – original draft, Writing – review & editing, Data curation, Formal analysis; **Ziwei Yao:** Methodology, Supervision, Writing – review & editing; **Wenjun Yao:** Investigation, Validation; **Yafang Li:** Investigation, Validation; **Gongbo Ma:** Formal analysis, Validation; **Meng Cui:** Investigation, Validation; **Nan Zheng:** Funding acquisition, Methodology, Supervision.

Acknowledgments

This work was supported by the Natural Science Foundation of Liaoning Province

https://doi.org/10.5194/egusphere-2026-6956
Preprint. Discussion started: 23 November 2026
© Author(s) 2026. CC BY 4.0 License.

(Doctoral Research Start-up Program, Grant No. 2026-BS-0883). Deepseek was used to assist with language editing and improve the clarity of author-written text during manuscript preparation. The authors reviewed the AI-assisted suggestions and take full responsibility for the final content of the manuscript.

References

Anderson, D.M., O'Connor, M.I. and Kremer, C.T. 2026. Trophic Interactions Influence Thermal Adaptation of Phytoplankton Size and Stoichiometry. Am. Nat. 207(2), 313-333.

Anderson, S.I., Barton, A.D., Clayton, S., Dutkiewicz, S. and Rynearson, T.A. 2021. Marine phytoplankton functional types exhibit diverse responses to thermal change. Nat. Commun. 12(1), 9.

Anderson, S.I., Franzè, G., Kling, J.D., Wilburn, P., Kremer, C.T., Menden-Deuer, S., Litchman, E., Hutchins, D.A. and Rynearson, T.A. 2022. The interactive effects of temperature and nutrients on a spring phytoplankton community. Limnol. Oceanogr. 67(3), 634-645.

Barton, S., Jenkins, J., Buckling, A., Schaum, C.E., Smirnoff, N., Raven, J.A. and Yvon-Durocher, G. 2020. Evolutionary temperature compensation of carbon fixation in marine phytoplankton. Ecol. Lett. 23(4), 722-733.

Becker, S., Aoyama, M., Woodward, E.M.S., Bakker, K., Coverly, S., Mahaffey, C., Tanhua, T. 2020. GO-SHIP Repeat Hydrography Nutrient Manual: The precise and accurate determination of dissolved inorganic nutrients in seawater, using Continuous

https://doi.org/10.5194/egusphere-2026-6956
Preprint. Discussion started: 23 November 2026
© Author(s) 2026. CC BY 4.0 License.



660 Flow Analysis methods. GO-SHIP/IOCCP, Paris.

661 Bi, R., Cao, Z., Ismar-Rebitz, S.M.H., Sommer, U., Zhang, H.L., Ding, Y. and Zhao,
662 M.X. 2021. Responses of Marine Diatom-Dinoflagellate Competition to Multiple
663 Environmental Drivers: Abundance, Elemental, and Biochemical Aspects. Front.
664 Microbiol. 12, 15.

665 Chen, B.Z. 2015. Patterns of thermal limits of phytoplankton. J. Plankton Res. 37(2),
666 285-292.

667 Chen, Y.J., Xu, M.Y., Wang, Y.H., Chen, H.L., Cheng, X.T., Ji, N.J., Zhou, L.J., Sun,
668 S. and Shen, X. 2025a. Physiological and molecular responses of the dinoflagellate
669 *Gymnodinium impudicum* to phosphorus deficiency: Insights into dissolved organic
670 phosphorus utilization strategies. Algal Res. 91, 10.

671 Chen, Z.J., Wang, Z.Q., Zeng, Z. and Tang, J.J. 2025b. Comparative Study on the
672 Diffusion of Thermal Discharge from Coastal Power Plants in Different Geographical
673 Environments. J. Mar. Sci. Eng. 13(2), 21.

674 Frank, F., Danger, M., Hillebrand, H. and Striebel, M. 2020. Stoichiometric
675 constraints on phytoplankton resource use efficiency in monocultures and mixtures.
676 Limnol. Oceanogr. 65(8), 1734-1746.

677 Gerhard, M., Koussoroplis, A.M., Hillebrand, H. and Striebel, M. 2019.
678 Phytoplankton community responses to temperature fluctuations under different
679 nutrient concentrations and stoichiometry. Ecology 100(11), 11.

680 Grasshoff, K., Kremling, K., Ehrhardt, M. 1999. Methods of Seawater Analysis, 3rd
681 ed. Wiley-VCH, Weinheim.

https://doi.org/10.5194/egusphere-2026-6956
Preprint. Discussion started: 23 November 2026
© Author(s) 2026. CC BY 4.0 License.



682 Guo, S.J., Wang, F., Yao, Q.Z., Wang, Y.Q., Feng, M.P. and Sun, X.X. 2025.
683 Seasonal dynamics and environmental drivers of phytoplankton carbon biomass in the
684 southern yellow sea. Cont. Shelf Res. 285, 14.
685 Happe, A., Ahme, A., Cabrerizo, M.J., Gerhard, M., John, U. and Striebel, M. 2024.
686 The experimental implications of the rate of temperature change and timing of
687 nutrient availability on growth and stoichiometry of a natural marine phytoplankton
688 community. Limnol. Oceanogr. 69(8), 1769-1781.
689 Holm-Hansen, O., Lorenzen, C.J., Holmes, R.W., Strickland, J.D.H. 1965.
690 Fluorometric determination of chlorophyll. Journal du Conseil / ICES Journal of
691 Marine Science 30, 3–15.
692 Isanta-Navarro, J., Peoples, L.M., Bras, B., Church, M.J. and Elser, J.J. 2024.
693 Elemental and macromolecular plasticity of *Chlamydomonas reinhardtii* (Chlorophyta)
694 in response to resource limitation and growth rate. J. Phycol. 60(2), 418-431.
695 Kholssi, R., Lougraimzi, H. and Moreno-Garrido, I. 2023. Effects of global
696 environmental change on microalgal photosynthesis, growth and their distribution.
697 Mar. Environ. Res. 184, 11.
698 Kontopoulos, D.G., van Sebille, E., Lange, M., Yvon-Durocher, G., Barraclough, T.G.
699 and Pawar, S. 2020. Phytoplankton thermal responses adapt in the absence of hard
700 thermodynamic constraints. Evolution 74(4), 775-790.
701 Kranzler, C.F., Krause, J.W., Brzezinski, M.A., Edwards, B.R., Biggs, W.P.,
702 Maniscalco, M., McCrow, J.P., Van Mooy, B.A.S., Bidle, K.D., Allen, A.E. and
703 Thamatrakoln, K. 2019. Silicon limitation facilitates virus infection and mortality of

https://doi.org/10.5194/egusphere-2026-6956
Preprint. Discussion started: 23 November 2026
© Author(s) 2026. CC BY 4.0 License.



marine diatoms. Nat. Microbiol 4(11), 1790-1797.

Lin, J., Zou, X.Q., Huang, F.M. and Yao, Y.L. 2021. Quantitative estimation of sea surface temperature increases resulting from the thermal discharge of coastal power plants in China. Mar. Pollut. Bull. 164, 9.

Liu, K.L., Nishioka, J., Chen, B.Z., Suzuki, K., Cheung, S., Lu, Y.H., Wu, H.J. and Liu, H.B. 2023. Role of nutrients and temperature in shaping distinct summer phytoplankton and microzooplankton population dynamics in the western North Pacific and Bering Sea. Limnol. Oceanogr. 68(3), 649-665.

Lysenko, V., Rajput, V.D., Singh, R.K., et al. 2022. Chlorophyll fluorometry in evaluating photosynthetic performance: key limitations, possibilities, perspectives and alternatives. Physiology and Molecular Biology of Plants 28, 2041–2056.

Maavara, T., Akbarzadeh, Z. and Van Cappellen, P. 2020. Global Dam-Driven Changes to Riverine N:P:Si Ratios Delivered to the Coastal Ocean. Geophys. Res. Lett. 47(15), 9.

Malone, T.C. and Newton, A. 2020. The Globalization of Cultural Eutrophication in the Coastal Ocean: Causes and Consequences. Front. Mar. Sci. 7, 30.

Marañón, E., Fernández-González, C. and Tarran, G.A. 2024. Effect of temperature, nutrients and growth rate on picophytoplankton cell size across the Atlantic Ocean. Sci Rep 14(1), 13.

Marie, D., Partensky, F., Jacquet, S., Vaulot, D. 1997. Enumeration and cell cycle analysis of natural populations of marine picoplankton by flow cytometry using the nucleic acid stain SYBR Green I. Applied and Environmental Microbiology 63,

https://doi.org/10.5194/egusphere-2026-6956
Preprint. Discussion started: 23 November 2026
© Author(s) 2026. CC BY 4.0 License.



186–193.

Ou, L.J., Wang, Z., Ding, G.M., Han, F.X., Cen, J.Y., Dai, X.F., Li, K.Q. and Lu, S.H. 2024. Organic nutrient availability and extracellular enzyme activities influence harmful algal bloom proliferation in a coastal aquaculture area. Aquaculture 582, 9.

Park, S., Kim, G., Kwon, H.K. and Han, I.S. 2023. Long-term changes in the concentrations of nutrients in the marginal seas (Yellow Sea, East China Sea, and East/Japan Sea) neighboring the Korean Peninsula. Mar. Pollut. Bull. 192, 6.

Thomas, M.K., Aranguren-Gassis, M., Kremer, C.T., Gould, M.R., Anderson, K., Klausmeier, C.A. and Litchman, E. 2017. Temperature-nutrient interactions exacerbate sensitivity to warming in phytoplankton. Glob. Change Biol. 23(8), 3269-3280.

Thyssen, M., Grégori, G., Créach, V., et al., 2023. Interoperable vocabulary for marine microbial flow cytometry. Frontiers in Marine Science 10, 1198093.

Tomas, C.R. (Ed.), 1997. Identifying Marine Phytoplankton. Academic Press, San Diego.

Tong, F., Chen, P.M. and Zhang, X.M. 2023. Dissolved Inorganic Nutrient Biogeochemistry in an Urbanized Coastal Region: A Study of Dapeng Cove, Shenzhen. Sustainability 15(24), 22.

Utermöhl, H.,1958. Zur Vervollkommnung der quantitativen Phytoplankton-Methodik. Mitteilungen der Internationalen Vereinigung für Theoretische und Angewandte Limnologie 9, 1–38.

Weng, C.S., Ding, D.S., Yang, Q., Zhu, L., Sun, J., Qu, K.M., Cui, Z.G. and Wei, Y.Q.

https://doi.org/10.5194/egusphere-2026-6956
Preprint. Discussion started: 23 November 2026
© Author(s) 2026. CC BY 4.0 License.



2025. Significance of temperature and salinity in the dynamics of diatoms and dinoflagellates along the coastal Yellow Sea. Prog. Oceanogr. 234, 10.

Xiao, W.P., Liu, X., Irwin, A.J., Laws, E.A., Wang, L., Chen, B.Z., Zeng, Y. and Huang, B.Q. 2018. Warming and eutrophication combine to restructure diatoms and dinoflagellates. Water Res. 128, 206-216.

Zhang, C., Yao, X.H., Chen, Y., Chu, Q., Yu, Y., Shi, J.H. and Gao, H.W. 2019. Variations in the phytoplankton community due to dust additions in eutrophication, LNLC and HNLC oceanic zones. Sci. Total Environ. 669, 282-293.

Zhang, X.S., Yu, K.L., Li, M., Jiang, H., Gao, W.M., Zhao, J. and Li, K.Q. 2024. Diatom-dinoflagellate succession in the Bohai Sea: The role of N/P ratios and dissolved organic nitrogen components. Water Res. 251, 12.

Zhao, J.Y., Kong, N., Sun, S.Q., Hao, W.T., Wang, B., Wang, L.L. and Song, L.S. 2026. Phosphorus and silicon starvation disrupts fatty acid balance in the diatom *Nitzschia closterium f. minutissima* and induces inflammatory responses in oyster larvae. Water Biol. Secur. 5(4), 8.

Zheng, B.F., Lucas, A.J., Franks, P.J.S., Schlosser, T.L., Anderson, C.R., Send, U., Davis, K., Barton, A.D. and Sosik, H.M. 2023. Dinoflagellate vertical migration fuels an intense red tide. Proc. Natl. Acad. Sci. U. S. A. 120(36), 6.

Zhou, Z.X., Yu, R.C. and Zhou, M.J. 2017. Seasonal succession of microalgal blooms from diatoms to dinoflagellates in the East China Sea: A numerical simulation study. Ecol. Model. 360, 150-162.